

Article

Combined Geometrical Optimisation of a Square Microchannel with Smoothed Corners

Marco Lorenzini ^{1,*}  and Nicola Suzzi ^{2,†}¹ Industrial Engineering Department—DIN, Alma Mater Studiorum, Università di Bologna, Forlì Campus, Via Fontanelle 40, 47121 Forlì, Italy² Dipartimento Politecnico di Ingegneria e Architettura (DPIA), Università degli Studi di Udine, Via delle Scienze 206, 33100 Udine, Italy; nicola.suzzi@uniud.it

* Correspondence: marco.lorenzini@unibo.it

† These authors contributed equally to this work.

Abstract: Several engineering systems currently use microchannel heat sinks. In order to increase the performance of these devices, optimisation according to the first and second law of thermodynamics is employed. One way to achieve the goal is to modify the geometry of the cross-section, as is done in this paper for square ducts, having the walls at a uniform temperature which is higher than that of the bulk fluid at the inlet. The effects of both the thermal entry region of the duct and the heat generation due to viscous dissipation are considered. The resulting Graetz–Brinkman problem is solved numerically to obtain the velocity and temperature fields. It is demonstrated that non-negligible viscous heating eventually causes the heat flux to reverse (from fluid to walls), and that, only after this condition is achieved, can the flow become fully developed, which makes the entry region the only useful stretch for real-life applications. The length after which the direction of the heat flux reverses due to viscous heating in the fluid is obtained as a function of the Brinkman number and of the smoothing radius. Optimisation with performance evaluation criteria and entropy generation minimisation was carried out separately, and the results were combined into a single objective function. A comparison with published models highlights how neglecting the entry region and viscous heating yields misleading results. It turns out that smoothing the corners is always profitable in the case of the constrained heated perimeter or area of the cross-section but seldom when the characteristic length or the hydraulic diameter is fixed. With few exceptions, viscous heating amplifies the trends experienced for zero-Brinkman flows. The results are in non-dimensional form, yet they have been obtained starting from plausible dimensional values and are applicable to real-life devices.

Keywords: microchannels; viscous heating; Graetz–Brinkman problem; entropy analysis; thermodynamic optimisation; performance evaluation criteria



Citation: Lorenzini, M.; Suzzi, N. Combined Geometrical Optimisation of a Square Microchannel with Smoothed Corners. *Energies* **2024**, *17*, 2666. <https://doi.org/10.3390/en17112666>

Academic Editor: Artur Blaszczyk

Received: 12 April 2024

Revised: 20 May 2024

Accepted: 28 May 2024

Published: 30 May 2024



Copyright: © 2024 by the authors. Licensee MDPI, Basel, Switzerland. This article is an open access article distributed under the terms and conditions of the Creative Commons Attribution (CC BY) license (<https://creativecommons.org/licenses/by/4.0/>).

1. Introduction

Microchannels are employed in a wide variety of engineering systems. The use of microchannel heat sinks belonging to the so-called MFDs (micro-flow devices) ranges from the integrated cooling of small electronic components to much larger assemblies, such as those for HVAC, and the trend seems to keep steadily increasing [1–4]. Advanced manufacturing techniques, often pioneered in the semiconductor industry, have opened up new possibilities for creating unique structures and channels with varying cross-sections, allowing the miniaturisation of geometries previously restricted to much larger dimensions [1,5–9]. This, in turn, has led to renewed interest in exploring laminar forced convection through channels of different shapes, as evidenced by numerous research studies [10–18]. These works investigate the fundamental phenomena driving fluid flow and heat transfer in single microchannels or in rows of microchannels forming a heat sink. At such small dimensional scales, effects like viscous dissipation [19] (which may also be present at the

scales usually associated with traditional pieces of equipment) can become non-negligible, mainly when liquid flows are involved. However, studies for viscous dissipation of gases and rarefied gases have been conducted [20–22]. Morini [10] presented a criterion to determine the limit of significance for viscous heating and modified correlations for the Nusselt number as a function of the Brinkman number. A similar problem was investigated numerically by Barletta and Magyari [23] for rectangular channels with either uniform heat flux or temperature at the walls, obtaining the Nusselt number for different aspect ratios of the channel.

Non-Newtonian fluids and nanofluids also exhibit a distinct behaviour when viscous dissipation is involved, and several studies have dealt with the problem for micro-geometries [11,24,25], also considering slip at the walls [26]; many results were obtained, which have been recently summarised in a review by Bayareh [27] covering non-Newtonian nanofluids; one of the most significant findings of the paper is that a single-phase description of the flow cannot provide accurate results owing to the change in the parameters of the fluid and that the distribution of nanoparticles in the fluid must be known.

Viscous dissipation has been studied in conjunction with other micro-effects such as rarefaction due to the reduction of the length scale [21,28]. Yet, this micro-effect tends to counteract the action of friction. This was demonstrated recently by Su and Yang [29], who analytically investigated the fully developed slip flow of a rarefied gas through elliptical microchannels with uniform heat flux and uniform circumferential temperature at the walls. The analysis pointed out, unsurprisingly, that gas rarefaction could significantly abate the negative influence of viscous dissipation on the Nusselt number. Another finding was that axial conduction, associated with a Peclet number lower than unity for this study dominates irreversibilities and masks all other contributions.

Contrary to rarefaction, Joule heating occurring for electro-osmotic flow, another micro-effect, adds to viscous dissipation: it can be considered an equivalent dissipation term even when viscous heating plays no role. Besides works of theoretical and numerical nature or experimental works on single channels [30–33], some papers exist where experimental prototypes of heat exchangers relying on EOF, and were realised by Al-Rjoub and co-workers [34,35]. The results indicated an increase in the Nusselt number for electro-osmotic flow with respect to an analogous pressure-driven flow, which was attributed to the difference in the velocity profiles (plug flow instead of parabolic flow). When Joule heating started to be significant, i.e., in the high range of the voltages applied, the Nusselt number decreased. In contrast, adding nanoparticles to the base fluid increased the energy transferred to the fluid per unit mass flow rate, albeit at the expense of a decrease in the flow rate.

In microchannels, given the characteristic lengths involved and the nature of the flow (predominantly laminar), the thermal entry region may occupy one significant portion of the total length, so that the assumption of fully developed flow is no longer appropriate. The determination of the temperature profile in the thermal entry region of channels and ducts is known as the Graetz problem, which was solved by Graetz and Prandtl more than a century ago. Over the years, the problem was extended to include axial conduction [36] and viscous dissipation [37]. The latter became known as the Graetz–Brinkman problem, and was also solved for parallel plates by Barletta and Magyari [23], who included a so-called thermal preparation length to account for the temperature profile induced by viscous dissipation in the flow. Extensions to other cross-sections were carried out by Aparecido and Cotta [38], Lee and Garimella [39], and Filiali et al. [40]. The investigation has been extended to microchannels through the solution of the micro-Graetz–Brinkman problem, in which axial conduction, viscous dissipation and rarefaction/slip are taken into account [7,23,41]; yet, these studies are restricted to basic geometries.

The discussion above highlights how microchannels are no longer mere subjects of fundamental research and are currently finding applications in engineering systems, although several areas of fundamental investigation remain. Several techniques are available to increase the heat duty and lower the mean temperature difference and the required

pumping power under given design constraints. These were developed for conventional heat exchangers, and are thoroughly reviewed in [42]. The need to assess the possible enhancement of performance induced by changes in the basic configuration has led to the introduction of performance evaluation criteria, PEC, [43,44], which treat the problem from the perspective of the first law of thermodynamics. Thanks to the works of Bejan [45–47] on entropy generation minimisation (EGM), awareness of the importance and potential of the second law in the analysis of the performance of heat exchangers grew, giving rise to several works and different techniques, a review of which can be found in [48]. More recently, researchers have dealt with the optimisation of micro heat exchangers [49–51] in terms of the first and second law, with new and interesting results obtained when conjugate effects are considered. An extensive body of work on the combined use of PEC and EGM has been produced by Zimparov, who extended the former method [52,53] and co-authored [54,55] with some recent contributions where the relative performance of different cross-sections under laminar flow conditions and either H or T boundary conditions are studied: see [56] for further references. Zimparov suggests [52,53] the use of ratios and products of the objective functions for the first- and second-law analysis to combine and relate their results: the underlying notion is that when the resulting quantity takes a value below unity, this indicates a configuration that performs better than the reference case.

Among the many shapes of the ducts of heat exchangers that have been investigated, square cross-sections with smoothed corners have recently been studied in two works [57,58] for laminar flow and H1 and H2 boundary conditions. In [58], the authors carry out an investigation of the comparative performance of the ducts relative to a circular tube (which corresponds to a radius of curvature equal to half the side of the square duct with sharp corners) according to first- and second-law analysis, applying different constraints on the geometrical parameters (fixed side a , fixed cross-sectional area, A_c , fixed hydraulic diameter, D_h , and fixed heated perimeter P_h). The results are presented in terms of normalised PEC quantities, namely heat duty, \dot{Q}^* , difference between wall and bulk temperature, ΔT^* , pumping power P^* and channel length L^* , and EGM-related quantities, such as augmentation entropy generation number, N_S , augmentation entropy generation rate due to heat transfer, N_T , and friction, N_P , for three values of the irreversibility distribution ratio ϕ_{ref} , which ranges from 10^{-3} to 10^{-1} . The comments of the authors on the results are based essentially on the analysis of the resulting plots, but there is only a cursory attempt to employ the underlying equations to explain the results. As a comparison is made, keeping the circular duct as reference, and results from PEC and EGM are kept separate, it is concluded that, for some cases, the entropy analysis is not appropriate for the investigation.

Lorenzini and Morini [59] and Lorenzini and Suzzi [60] analysed microchannels with square, rectangular and trapezoidal shapes with smoothed corners for the case of the fully developed flow and uniform heat flux along the channel length and perimeter and uniform temperature over the heated perimeter of the cross-section both with and without viscous dissipation. The correlations obtained for the Poiseuille and Nusselt numbers were then used in [60] to carry out an optimisation based on the use of both first- and second-law approaches. Results were interpreted in light of the changes in the geometry and of the underlying model equations.

In this paper, the optimisation of microchannels of a square cross-section with smoothed corners and uniform temperature imposed at the walls is carried out using both PEC and EGM. The flow is thermally developing, and cases with viscous dissipation, as exemplified by the Brinkman number, Br , are considered, namely for $Br = 10^{-3}$ and $Br = 10^{-2}$: these values are representative of real-life operating conditions. The Poiseuille number is obtained from a previous work by the same authors [17]. The Nusselt number is expressed as a function of the fully-developed Nusselt number when viscous heating dominates and of the Nusselt number for developing flow and negligible viscous heating, of the Brinkman number, and of a coefficient that depends on the non-dimensional smoothing radius.

A criterion is established to determine the critical length of the microchannel, \tilde{x}_{cr} , the one past which viscous heating starts to reverse the heat flux (from the fluid to the walls), and its dependence on the Brinkman number and on the smoothing radius is given.

It is proved that the correlation proposed for the average Nusselt number, \bar{Nu} , when viscous heating and entry region are considered, is in outstanding agreement with the numerical results for the whole stretch of the channel length up to $\tilde{x}_{cr}1$, which is the maximum useful length of the channel. Optimisation is carried out considering the various PEC applicable here, and an entropy balance yields the quantities needed to compute the entropy generation number (EGN), which comes from the sum of the contributions due to fluid flow and heat transfer. The results are compared to those obtained by other authors who only considered the contribution of fully developed flow to highlight the discrepancies. In order to enclose both approaches in the optimisation, a combined objective function is defined suitably for each optimisation problem studied—which corresponds to a different PEC—and the results are presented in graphical form and commented throughout. The results are presented in non-dimensional form to offer both conclusions of general validity and a versatile tool for design applications, but the values are obtained starting from actual dimensional quantities and can, therefore, be employed confidently in practical applications.

2. Mathematical Model

2.1. Performance Evaluation Criteria

Performance evaluation criteria (PEC) are used for heat exchanger design. PEC are based on the first law of thermodynamics and are characterised by the objective functions: total heat flux q , temperature difference between the solid wall and fluid bulk through the inlet section ΔT_i , pumping power W , channel length L , and mass flow rate \dot{m} . Depending on the applied PEC, one of the objective functions must be maximised or minimised, while some constraints are applied to the others, as shown in the table below. Starred quantities in Table 1 are non-dimensional and correspond to the ratio of the value for the objective function of the modified configuration to the same value for the reference case (here, the cross-section with sharp corners). Unit values indicate that the quantity is constrained to being unchanged, whilst the arrows show whether the objective function should be minimised (arrow pointing downwards) or maximised (arrow pointing upwards).

Table 1. Performance evaluation criteria.

Criteria	q^*	ΔT^*	W^*	L^*	\dot{m}^*
FG1a	↑	1		1	1
FG1b	1	↓		1	1
FG2a	↑	1	1	1	
FG2b	1	↓	1	1	
VG2a	↑	1	1		1
VG2b	1	↓	1		1

The PEC require two equations: the energy balance, which links the heat flux to ΔT_i , L , and \dot{m} ; and the pumping power, derived from the pressure drop, which depends on L and \dot{m} .

Following [61], the energy balance for a control volume of the channel with length δx and volume $\delta V = \delta x A_c$ gives,

$$\dot{m} c_p \frac{dT_b}{dx} = \alpha P (T_w - T_b) + \dot{q}_v A_c \quad (1)$$

where \dot{q}_v is the heat source deriving from viscous heating, A_c is the cross-section area and P is the cross-section perimeter. Imposing the temperature T_w at the solid wall of the channel and denoting the difference between wall temperature and fluid bulk temperature

as $\Delta T = T_w - T_b$, the energy balance can be integrated along the channel axis, giving the bulk temperature profile [61]:

$$\Delta T = \left(\Delta T_i + \frac{\dot{q} A_c}{\bar{\alpha} P} \right) \exp \left(-\frac{\bar{\alpha} P x}{\dot{m} c_p} \right) - \frac{\dot{q}_v A_c}{\bar{\alpha} P} \quad (2)$$

$\bar{\alpha}$ being the average heat transfer coefficient and ΔT_i the temperature difference between the solid wall and the bulk fluid entering the channel. Integrating the heat flux per unit length along the channel allows to calculate the global heat flux,

$$q = \bar{\alpha} P \int_0^L \Delta T dx \quad (3)$$

Substituting Equation (2) for ΔT into Equation (3) yields [61],

$$q = \dot{m} c_p \Delta T_i \left(1 + \frac{\dot{q} A_c}{\bar{\alpha} P \Delta T_i} \right) \left[1 - \exp \left(-\frac{\bar{\alpha} P L}{\dot{m} c_p} \right) \right] - \dot{q}_v A_c L \quad (4)$$

Introducing the non-dimensional viscous dissipation function Φ , the viscous heating term can be recast as

$$\dot{q} = \frac{\mu u_b^2}{D_h^2} \Phi, \quad \text{with} \quad \Phi = 2 \frac{A_c}{D_h^2} \text{Po} \quad (5)$$

where u_b is the fluid bulk velocity, D_h is the cross-section hydraulic diameter, and Po is the Poiseuille number, that is, the product of the Reynolds number, Re, times the friction factor, f :

$$\text{Po} = f \text{Re}, \quad \text{with} \quad \text{Re} = \frac{\rho u_b D_h}{\mu} \quad (6)$$

Following [60,61], the pumping power, which depends on the fluid flow rate and on the pressure drops, $W = \dot{m} \Delta p / \rho$, can be calculated as

$$W = \frac{2 \mu \dot{m}^2 L \text{Po}}{\rho^2 A_c D_h^2} \quad (7)$$

In practical applications, it is useful to normalise the objective functions with the reference values, corresponding to the base configuration to be optimised:

$$q^* = \frac{q}{q_0}, \quad \Delta T^* = \frac{\Delta T_i}{\Delta T_{i,0}}, \quad W^* = \frac{W}{W_0}, \quad L^* = \frac{L}{L_0}, \quad \dot{m}^* = \frac{\dot{m}}{\dot{m}_0} \quad (8)$$

Further introducing the Brinkman number, Br, the Peclet number, Pe, and the Nusselt number, Nu,

$$\text{Br} = \frac{\mu u_b^2}{\lambda \Delta T_i}, \quad \text{Pe} = \text{Re} \text{Pr}, \quad \text{Pr} = \frac{\mu c_p}{\lambda}, \quad \text{Nu} = \frac{\alpha D_h}{\lambda} \quad (9)$$

Equations (4) and (7) can be rewritten in non-dimensional form:

$$q^* = \dot{m}^* \Delta T^* \frac{(1 - e^{-A})(1 + B) - A B}{(1 - e^{-A_0})(1 + B_0) - A_0 B_0} \quad (10)$$

$$A = 4 \frac{\overline{\text{Nu}}}{\text{Pe}} \frac{L}{D_h}, \quad B = \frac{1}{2} \frac{\text{Br} \text{Po}}{\overline{\text{Nu}}} \frac{A_c}{D_h^2} \quad (11)$$

$$W^* = \frac{W}{W_0} = \frac{\dot{m}^{*2} L^* \text{Po}^*}{A_c^* D_h^{*2}} \quad (12)$$

It is important to point out that both the Peclet number and the Brinkman number can be expressed as an explicit function of both the PEC objective functions and the channel geometry:

$$\text{Pe} = \frac{c_p \dot{m} D_h}{\lambda A_c}, \quad \text{Br} = \frac{\mu \dot{m}^2}{\rho^2 \lambda A_c^2 \Delta T_i} \quad (13)$$

The aim of this paper is to optimise the geometry of a microchannel heat sink. A channel characterised by a rectangular cross-section with smoothed corners, such as the one in Figure 1, is considered and the effect of rounding the corners is investigated. Introducing the channel aspect ratio, β , and the non-dimensional smoothing radius, γ ,

$$\beta = \frac{b}{a} \in [0, 1], \quad \gamma = \frac{2r}{b} \in [0, 1] \quad (14)$$

the cross-section area, the cross-section perimeter, and the hydraulic diameter can be expressed as a function of β and γ :

$$A_c = a^2 \left[\beta - \left(\frac{\beta\gamma}{2} \right)^2 (4 - \pi) \right], \quad P = 2a \left[1 + \beta - \frac{\beta\gamma}{2} (4 - \pi) \right], \quad (15)$$

$$D_h = \frac{4A_c}{P} = a \frac{4\beta - (\beta\gamma)^2(4 - \pi)}{2(1 + \beta) - \beta\gamma(4 - \pi)}$$

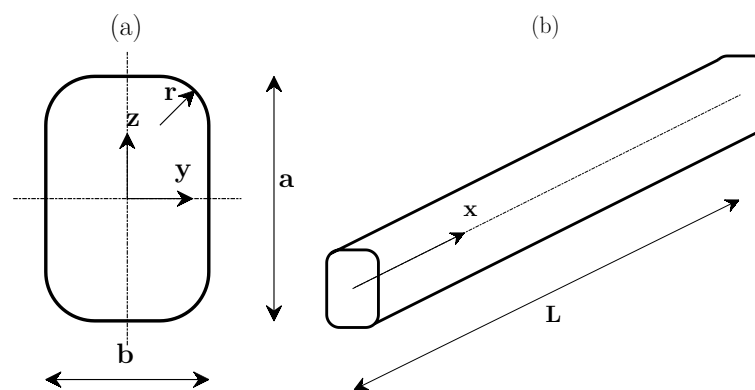


Figure 1. Channel cross-section geometry and Cartesian coordinate system: cross section (a); channel axis (b). For microchannels, the hydraulic diameter of the cross-section usually ranges between $0 \div 200 \mu\text{m}$.

Following [60], one further geometrical constraint must be imposed when γ is changed, and this can take one of four different forms: constant side length, $a/a_0 = 1$; or constant hydraulic diameter, $D_h/D_{h,0} = 1$; constant cross-section perimeter, $P/P_0 = 1$; constant cross-section area, $A_c/A_{c,0} = 1$. The sharp corner geometry ($\gamma_0 = 0$) is chosen as the reference configuration, and the resulting expressions of the normalised length of the base side a are reported in Table 2.

Table 2. Geometric constraints applied to the problem.

Constraint	$a^* = a/a_0$
$a = \text{const}$	$a^* = 1$
$D_h = \text{const}$	$a^* = \frac{2\beta}{1+\beta} \frac{2(1+\beta) - \beta\gamma(4-\pi)}{4\beta - (\beta\gamma)^2(4-\pi)}$
$P = \text{const}$	$a^* = \frac{2(1+\beta)}{2(1+\beta) - \beta\gamma(4-\pi)}$
$A_c = \text{const}$	$a^* = \frac{4\beta}{4\beta - (\beta\gamma)^2(4-\pi)}$

2.2. Entropy Generation Number

As PEC are based on the first law of thermodynamics, the entropy generation number (EGN) [46], a non-dimensional quantity related to the entropy generation rate and, thus, to the second law, is also considered for the combined optimisation of the channel geometry. Writing the entropy balance for a control volume $\delta V = A_c \delta x$ yields

$$d\dot{S} = \dot{m} ds - \frac{q' dx}{T_w}, \quad ds = c_p \frac{dT}{T} - \frac{dp}{\rho T} \quad (16)$$

The entropy generation rate $d\dot{S}$ is the sum of one contribution from heat transfer and one from the pressure drop:

$$d\dot{S} = d\dot{S}_T + d\dot{S}_P, \quad (17)$$

$$d\dot{S}_T = \dot{m} c_p \frac{dT}{T} - \frac{q' dx}{T_w}, \quad d\dot{S}_P = -\frac{\dot{m}}{\rho T} dp \quad (18)$$

Integrating the entropy generation rate from heat transfer along the channel length gives

$$\dot{S}_T = \int_0^L \frac{d\dot{S}_T}{dx} dx = \dot{m} c_p \left[\log\left(\frac{T_o}{T_i}\right) - \frac{T_o - T_i}{T_w} \right] + \frac{\dot{q}_v A_c L}{T_w} \quad (19)$$

with T_i being the inlet fluid temperature and T_o the outlet fluid temperature. Assuming $T_o/T_i \sim 1$ and expressing the fluid temperature as $T = T_w - \Delta T$, with ΔT being given as a function of x by Equation (2), the entropy generation rate due to heat transfer reduces to

$$\dot{S}_T = \dot{m} c_p \frac{\Delta T_i^2}{T_w (T_w - \Delta T_i)} \left(1 + \frac{\dot{q}_v A_c}{\bar{\alpha} P \Delta T_i} \right) \left[1 - \exp\left(-\frac{\bar{\alpha} P L}{\dot{m} c_p}\right) \right] + \frac{\dot{q}_v A_c L}{T_w} \quad (20)$$

Substituting the expression of the heat flux, Equation (4), into Equation (20) yields an alternative expression for the entropy generation rate due to heat transfer:

$$\dot{S}_T = \frac{q \Delta T_i}{T_i T_w} + \frac{\dot{q}_v A_c L}{T_i} \quad (21)$$

which is similar to the formulations published in the literature [52,53], but an additional term arises due to the effect of viscous heating.

The entropy generation number due to heat transfer N_T is calculated via normalisation of \dot{S}_T , Equation (20), with the reference value

$$N_T = \frac{\dot{S}_T}{\dot{S}_{T,0}} = \dot{m}^* \Delta T^* \frac{\Delta T^* (C_T - \Delta T^*)^{-1} (1 - e^{-A}) (1 + B) + A B}{(C_T - 1)^{-1} (1 - e^{-A_0}) (1 + B_0) + A_0 B_0} \quad (22)$$

where A , B are defined in Equation (11) and C_T is a non-dimensional parameter, corresponding to the ratio between the wall temperature and the reference inlet temperature difference:

$$C_T = \frac{T_w}{T_w - T_{i,0}} = \frac{T_w}{\Delta T_{i,0}} \quad (23)$$

The integration of the entropy generation rate caused by the pressure drop gives [60]:

$$\dot{S}_P = \int_0^L \frac{d\dot{S}_P}{dx} = \frac{2 \mu \dot{m}^2 L \text{Po}}{\rho^2 A_c D_h^2 T_w} \quad (24)$$

$$N_P = \frac{\dot{S}_P}{\dot{S}_{P,0}} = \frac{\dot{m}^{*2} L^* \text{Po}^*}{A_c^* D_h^{*2}} \quad (25)$$

where N_P is the entropy generation number due to pressure drop and Po^* is obtained normalising the Poiseuille number with its reference value. It should be noted that Equation (25) is equivalent to Equation (12), which refers to the calculation of the normalised pumping power. The entropy generation number N_S is calculated combining N_T and N_P :

$$N_S = \frac{N_T + \phi N_P}{1 + \phi}, \quad \phi = \frac{\dot{S}_{P,0}}{\dot{S}_{T,0}} \quad (26)$$

2.3. Graetz–Brinkman Problem

The solution of the Graetz–Brinkman problem gives the velocity field and the temperature field inside the channel, which, in turn allows, the calculation of the Poiseuille number and of the local Nusselt number, both required to estimate the entropy generation rate and the objective function of any PEC. The velocity and the temperature fields along the thermal entry region were numerically computed in [17] by solving the governing Navier–Stokes equations. We consider a fluid flowing through a channel of constant cross-section along the axial direction x , such as the one of Figure 1, and assume stationary condition, incompressible, Newtonian fluid, hydrodynamically developed flow, laminar regime, and negligible axial conduction. Introducing the following non-dimensional quantities:

$$\tilde{x} = \frac{1}{\text{Pe}} \frac{x}{D_h}, \quad \tilde{y} = \frac{y}{D_h}, \quad \tilde{z} = \frac{z}{D_h}, \quad \tilde{u} = \frac{u}{u_b}, \quad \Theta = \frac{T - T_w}{T_w - T_i}, \quad \Phi = \left(\frac{\partial \tilde{u}}{\partial \tilde{y}} \right)^2 + \left(\frac{\partial \tilde{u}}{\partial \tilde{z}} \right)^2 \quad (27)$$

the Navier–Stokes equations can be recast in non-dimensional form:

$$\frac{\partial^2 \tilde{u}}{\partial \tilde{y}^2} + \frac{\partial^2 \tilde{u}}{\partial \tilde{z}^2} + 2 \text{Po} = 0 \quad (28)$$

$$\tilde{u} \frac{\partial \Theta}{\partial \tilde{x}} = \frac{\partial^2 \Theta}{\partial \tilde{y}^2} + \frac{\partial^2 \Theta}{\partial \tilde{z}^2} + \text{Br} \Phi \quad (29)$$

The Partial Differential Equation Toolbox provided in MATLAB® 2016a was used in [17] to solve Equations (28) and (29). Following [23], an adiabatic preparation of the fluid was imposed after the inlet section, allowing the assumption of a fully developed velocity profile, while a uniform temperature was imposed at the solid wall of the channel:

$$T|_{x=0} = T_i + T_\mu(y, z), \quad \Theta|_{\tilde{x}=0} = -1 + \Theta_\mu(\tilde{y}, \tilde{z}) \quad (30)$$

$$T|_{\partial\Omega} = T_w, \quad \Theta|_{\partial\Omega} = 0 \quad (31)$$

with Ω denoting the channel cross-section and Θ_μ being the local temperature increment due to viscous heating after the adiabatic preparation of the fluid. The temperature field was decomposed into $\Theta = \Theta_\mu + \Theta_0$, Θ_μ being the solution of the fully developed temperature field at dominant viscous heating, which is \tilde{x} —independent, and Θ_0 is the solution of the Graetz problem at $\text{Br} = 0$. Separating variables, Θ_0 was expressed as $\Theta_0 = \sum_n C_n \exp(-\lambda_n \tilde{x}) \Psi_n(\tilde{y}, \tilde{z})$, with λ_n being the eigenvalues and Ψ_n being the eigenfunctions. Thus, the 3D physical problem was reduced to a 2D mathematical problem. The numerical model was verified with literature numerical data [38] and validated with experimental evidence from [62] in terms of the Nusselt number along the thermal entry region, for a laminar flow in a rectangular channel with imposed wall temperature and negligible viscous heating. A detailed description of both the numerical method and the validation procedure is given in [17]. Running parametric computations, the local Nusselt number along the channel axial direction was correlated with the cross-section geometry and to the channel length [17],

$$\text{Nu} = \frac{\text{Nu}_0 - \text{Nu}_\mu \text{Br} \exp(b \tilde{x})}{1 - \text{Br} \exp(b \tilde{x})} \quad (32)$$

where \tilde{x} is the non-dimensional axial coordinate, defined in Equation (27), Nu_0 is the local Nusselt number deriving from the solution of the Graetz problem for $\text{Br} = 0$ (negligible viscous heating) and Nu_μ is the fully developed Nusselt number for $\text{Br} > 0$. The average Nusselt number can be obtained by integrating Equation (32) along the channel length,

$$\overline{\text{Nu}} = \frac{1}{\tilde{x}} \int_0^{\tilde{x}} \text{Nu} d\tilde{x} = \overline{\text{Nu}}_0 + \frac{1}{b \tilde{x}} \log \left[\frac{1 - \text{Br} \exp(b \tilde{x})}{1 - \text{Br}} \right] (\text{Nu}_\mu - \overline{\text{Nu}}_0) \quad (33)$$

$$\overline{\text{Nu}}_0 = \frac{1}{\tilde{x}} \int_0^{\tilde{x}} \text{Nu}_0 d\tilde{x} = a_0 + \frac{1}{a_1 \tilde{x}^n + a_2} \quad (34)$$

where the correlation for $\overline{\text{Nu}}_0$ was proposed by Lee and Garimella [39].

The coefficients a_0, a_1, a_2, b , required by Equations (33) and (34), depend on the channel cross-section geometry as well. As such coefficients are available in [17] for few channel configurations, they have to be determined as a function of the channel geometry running further computations, see Section 3.1. On the other hand, the Poiseuille number and the fully developed Nusselt number for $\text{Br} > 0$, which depend on the channel cross-section geometry, had been computed in [17] for many values of β, γ and correlated with γ via the following polynomial functions:

$$\text{Po} = \sum_{k=0}^4 c_k \gamma^k, \quad \text{Nu}_\mu = \sum_{k=0}^4 d_k \gamma^k \quad (35)$$

where the coefficients c_k, d_k are shown in Table 3 for $\beta = 1$. Values of c_k, d_k are available in [17] for a wide range of the aspect ratio β , in the case of rectangular channel with four rounded corners and whole cross-section perimeter heated and rectangular channel with two rounded corners and three sides heated, one side adiabatic.

Table 3. Polynomial coefficients of Equation (35).

Po		Nu	
c_0	+14.23	d_0	+7.949
c_1	+6.278	d_1	+3.613
c_2	−9.030	d_2	−1.955
c_3	+6.157	d_3	−0.5454
c_4	−1.629	d_4	+0.5408

3. Results

3.1. Nusselt Number Correlation

The numerical model developed in [17], which relies on the Partial Differential Equation Toolbox provided by MATLAB[®], was used to solve Equations (28) and (29) at different values of Br and γ , while the aspect ratio was kept at $\beta = 1$. Then, the computed temperature field was used to calculate the average Nusselt number $\overline{\text{Nu}}$ along the channel axis. The numerical model has already been validated with experimental evidences and verified with literature numerical data in [17]: in particular, the Graetz problem was numerically solved for a laminar flow in a channel having a rectangular cross-section with sharp corners and the computed Nusselt number along the thermal entry region successfully compared with [38,62]. As proved in [17], a triangular mesh characterised by a maximum distance between neighbour nodes set to $\Delta = 5 \times 10^{-3}$ elements suffices to ensure grid independence. Taking advantage of the geometrical symmetry of the problem, only 1/4 of the channel was solved. Computations at $\text{Br} = 0, 10^{-3}, 10^{-2}$ were run assuming laminar flow, and the following values of the non-dimensional smoothing radius were investigated: $\gamma = 0, 1/10, 1/5, 3/10, 2/5, 1/2, 3/5, 7/10, 4/5, 9/10$, and 1. Computations at negligible viscous heating ($\text{Br} = 0$) allowed the estimation of the coefficients a_0, a_1, a_2 , required by Equation (34), while computations at $\text{Br} > 0$ allowed the correlation of the coefficient b to the geometry of the channel cross-section. Two values of $\text{Br} > 0$ were studied to prove that b is independent of the value of the Brinkman number.

The fully developed velocity and temperature fields are shown in Figure 2. It is worth pointing out that the developed fluid temperature is higher than the imposed wall temperature, due to the heat generation induced by viscous heating: this, in practice, prevents the flow within the channels of a heat sink to be fully developed. In other words, when the wall temperature is fixed, viscous dissipation eventually causes the fluid to be warmer than the walls if the channel is long enough. This observation is a further testament to the importance of the entry region in microchannel heat sinks. Figure 3a shows the temperature field computed across the sections obtained by cutting the channel with the plane $y = 0$ and $y = z$, in the case of $\beta = 1, \gamma = 1/2$, and $\text{Br} = 10^{-2}$. The sectioning

plane is shown in Figure 2b by a dashed line. The goodness of the correlation for the average Nusselt number is proved by Figure 3b, where Equation (33) is compared with the numerical data. An outstanding agreement is observed before viscous heating supersedes the heat transfer from the channel walls (i.e., the fluid bulk temperature becomes higher than the imposed wall temperature), with a disagreement lower than 1% observed along the channel axis. It should be noted that the Nusselt number is somewhat underestimated when viscous heating dominates the heat transfer process. Nonetheless, the purpose here is the transfer of thermal energy from the walls to the bulk fluid, and the device ceases to be useful when it is the fluid that heats the channel walls. On this account, it is also relevant to introduce a threshold value, called critical length, L_{cr} , as the value that gives $T_b = T_w$, corresponding to the vertical asymptote in Figure 3b. In the optimisation, it is required that L be shorter than L_{cr} when optimising the microchannel geometry.

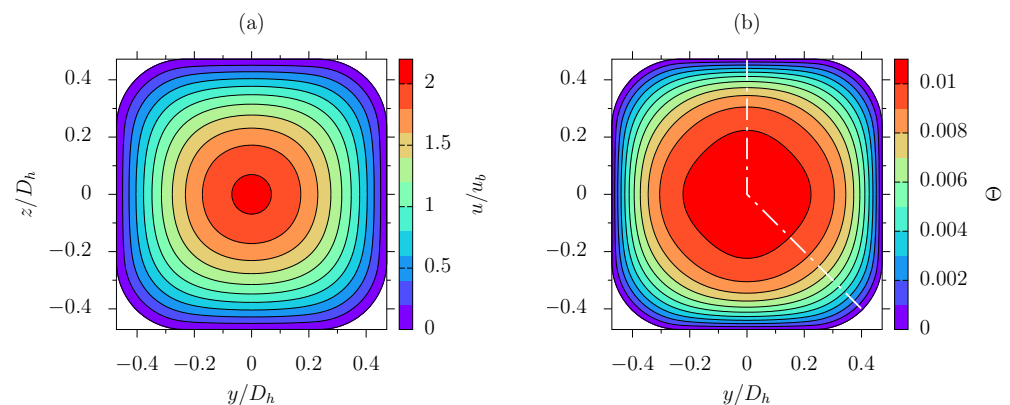


Figure 2. Fully developed velocity field (a) and fully developed temperature field (b) through the channel cross-section. $\beta = 1$, $\gamma = 1/2$, $Br = 10^{-2}$. The dashed line denotes the channel section used to plot temperature over the entry region in Figure 3a.

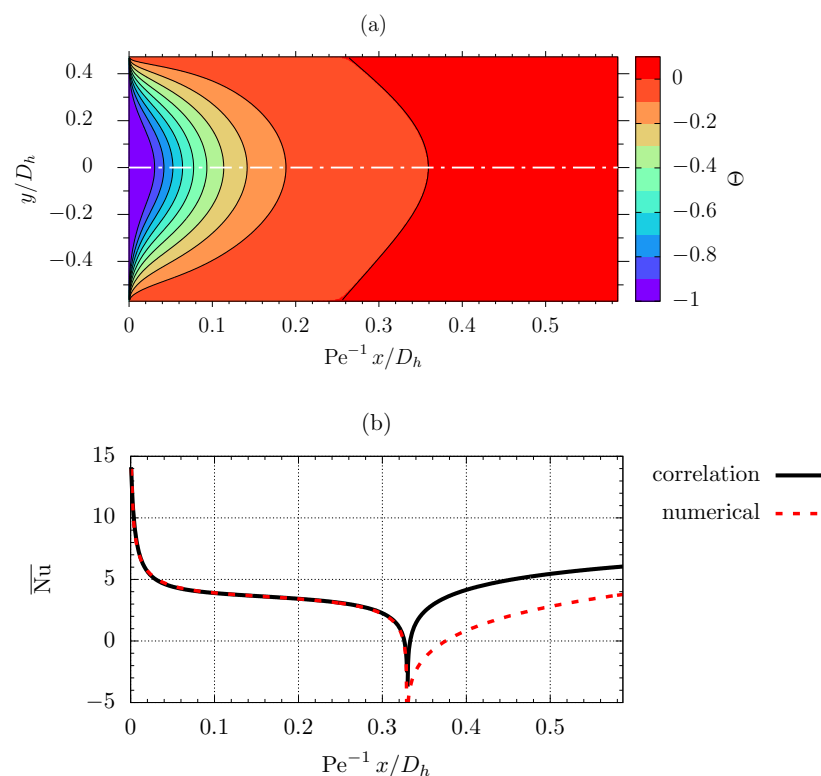


Figure 3. Non-dimensional temperature profile across sections $y = 0$ (above the white dotted line) and $y = z$ (below the white dotted line) (a); comparison between the computed average Nusselt number along the channel axis and the correlation proposed, Equation (33) (b). $\beta = 1$, $\gamma = 1/2$, $Br = 10^{-2}$.

Computing the coefficients a_0 , a_1 , a_2 , and b require to obtain the average Nusselt number, Equations (33) and (34), and applying a polynomial fit; such coefficients were fitted to the non-dimensional rounding radius γ for $\beta = 1$:

$$a_j = \sum_{k=0}^5 a_{jk} \gamma^k \text{ for } j = 0, 1, 2; \quad b = \sum_{k=0}^5 b_k \gamma^k \quad (36)$$

with the coefficients listed in Table 4.

Table 4. Polynomial coefficients of Equation (36) for $\beta = 1$.

a_0		a_1		a_2		b	
a_{00}	+2.9776	a_{10}	+18.362	a_{20}	+0.090502	b_0	+11.962
a_{01}	+1.3312	a_{11}	−0.95114	a_{21}	−0.034232	b_1	+5.3805
a_{02}	−0.43592	a_{12}	−1.2194	a_{22}	+0.071674	b_2	−3.1826
a_{03}	−0.39715	a_{13}	+18.575	a_{23}	−0.081391	b_3	+0.054179
a_{04}	+0.20136	a_{14}	−24.351	a_{24}	+0.044675	b_4	+0.262206
a_{05}	0	a_{15}	+9.0426	a_{25}	−0.008661	b_5	0

Figure 4 compares the non-dimensional critical length as a function of the non-dimensional smoothing radius predicted by the correlation,

$$\tilde{x}_{cr} = -\frac{\log(\text{Br})}{b} \quad (37)$$

which is derived from the numerical computations. Again, an excellent agreement is observed for both $\text{Br} = 10^{-2}$ and $\text{Br} = 10^{-3}$; it can, therefore, be concluded that, for practical purposes, the coefficient b is independent of the Brinkman number.

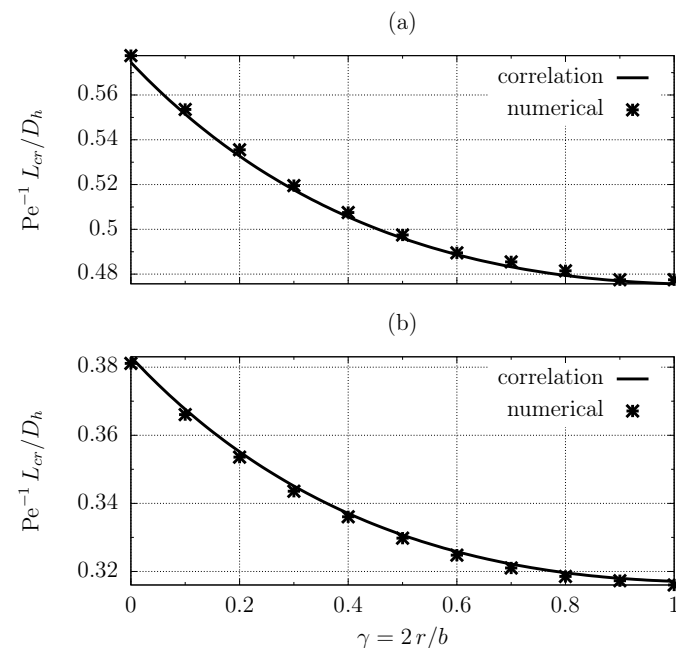


Figure 4. Computed critical length for the square microchannels as a function of smoothing radius versus correlation: $\text{Br} = 10^{-3}$ (a); $\text{Br} = 10^{-2}$ (b).

3.2. Microchannel Geometry Optimisation

The effect of rounding the corners of the reference square geometry of the channel cross-section is investigated next. The channel aspect ratio is set to $\beta = 1$, while the non-dimensional smoothing radius is changed, with the reference configuration being defined by sharp corners, which means $\gamma_0 = 0$.

The consistency of Equations (10) and (20), which gives the heat flux and the entropy generation number due to heat transfer in presence of viscous heating, coupled with the updated correlation for the average Nusselt number, which further includes the thermal entry region, are firstly investigated. To do so, it is shown that the present modellisation collapses to the one of [52], which can be used for the optimization of a standard heat exchanger, if the viscous heating is neglected (which is a valid approximation in most of the cases, but may give inaccurate results for microchannels). Indeed, assuming that $Br = 0$, the energy balance and the entropy generation balance, Equations (4) and (20) reduce to

$$q = \dot{m} c_p \Delta T_i (1 - e^{-A}), \quad q^* = \dot{m}^* \Delta T^* \frac{1 - e^{-A_0}}{1 - e^{-A_0}}, \quad A = 4 \frac{\overline{Nu}}{Pe} \frac{L}{D_h} \quad (38)$$

$$\dot{S}_T = \frac{q \Delta T_i}{T_w T_i}, \quad N_T = q^* \Delta T^* \frac{C_T - 1}{C_T - \Delta T^*} \quad (39)$$

which is similar to the formulation proposed by [52] for the modellisation of the heat transfer through ducts with constant wall temperature. The FG2b criterion (fixed pumping power, channel length, and heat flux) is considered next, using Equations (38) and (39) to derive the inlet temperature difference ΔT^* , which is the objective function of the FG2b criterion, and the entropy generation number due to heat transfer N_T as a function of the geometry of the channel cross-section. Results are compared with those obtained by the implementation of the model described in [52], which further assumes a fully developed flow. Three different test cases, listed in Table 5, are investigated. The test cases only differ in the imposed mean flow velocity, which ranges between 0.1 m/s and 1 m/s, resulting in different values of the reference Peclet number. It is important to point out that the test cases of Table 5 are consistent with practical applications involving microchannels. Since the flow inside the channel is laminar, this condition was implemented into the numerical procedure of [52], which uses the Blasius correlation and the Dittus–Boelter correlation to estimate the friction factor and the Stanton number for a fully developed, turbulent flow, using instead the correlations derived for a laminar, fully developed flow with constant wall temperature. Thus, the friction factor is derived from the Poiseuille number $Po = f Re$, given by Equation (35), while the Stanton number $St = Nu/Pe$ is derived from the fully developed Nusselt number in the case of negligible viscous heating,

$$Nu_\infty = \sum_{k=0}^5 a_{0k} \gamma^k \quad (40)$$

with the coefficients a_{0k} being given in Table 4 for $\beta = 1$.

Table 5. Reference configurations. Liquid water properties are evaluated at $p = 101,325$ Pa and $T = (T_w + T_i)/2$; the Brinkman number is set to $Br = 0$ (i.e., viscous heating is neglected).

Test Case	β	γ_0	L_0 (mm)	$D_{h,0}$ (mm)	u_0 (m/s)	T_w (°C)	$T_{i,0}$ (°C)	C_T	Pe_0
(a)	1	0	10	0.2	0.1	35	15	15.4	137.5
(b)	1	0	10	0.2	0.316	35	15	15.4	434.4
(c)	1	0	10	0.2	1	35	15	15.4	1375

The normalised inlet temperature difference and the entropy generation number due to heat transfer were traced as a function of the smoothing radius, applying the geometrical constraints of Table 2. The inlet temperature difference predicted by the present model and by the one of [52] is shown in Figure 5 for the test cases listed in Table 5, when the FG2b criterion is applied. It can be observed that the predicted ΔT^* collapses to the one of [52] at low Peclet numbers, see Figure 5a, meaning that the entry region length is negligible compared to the channel length, while results diverge at higher values of Pe , see Figure 5b,c. Indeed, increasing u_0 and, thus, the Peclet number, means that the length of the thermal entry region increases as well. Assuming a fully developed flow as in [52] yields that

the inlet temperature difference can always be reduced by smoothing the corners of the reference section for the test case (c), corresponding the to the highest Peclet number, while smoothing the corners is only convenient under the restriction applied on the cross-section perimeter P if the average Nusselt number, including the contribution of the thermal entry region, is employed.

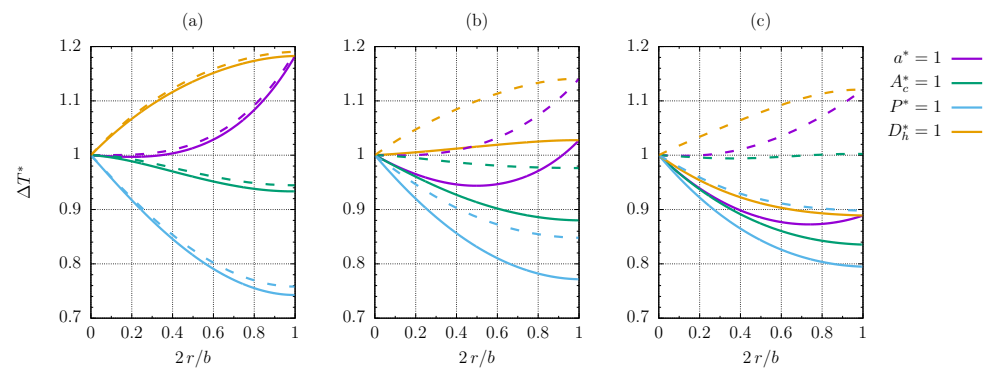


Figure 5. Normalised inlet temperature difference as a function of the smoothing radius: $Pe_0 = 137.5$ (a); $Pe_0 = 434.5$ (b); $Pe_0 = 1375$ (c). Continuous lines are derived from implementation of the model of [52], while dashed lines refer to the present model. FG2b criterion, $Br = 0$.

The same considerations are valid for the predicted entropy generation number due to heat transfer, see Figure 6. Again, it is concluded that the solution of the entropy balance is consistent with the literature [52], when viscous dissipation is negligible. This preliminary analysis demonstrates the consistency of the proposed modellisation, as it collapses to the one of [52], when the effects of the thermal entry region and of the viscous heating are neglected. Furthermore, Figures 5c and 6c prove that an accurate prediction of the heat transfer performance of a microchannel requires the modellisation of the thermal entry region, usually negligible in the presence of a turbulent flow.

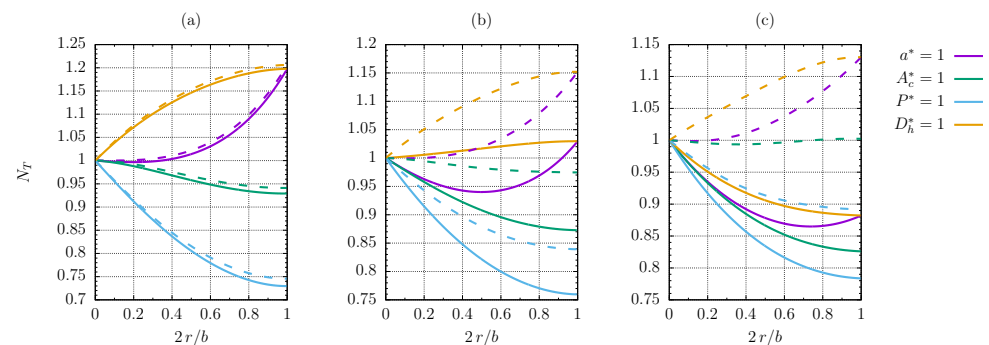


Figure 6. Entropy generation number due to heat transfer as a function of the smoothing radius: $Pe_0 = 137.5$ (a); $Pe_0 = 434.5$ (b); $Pe_0 = 1375$ (c). Continuous lines are derived from implementation of the model of [52], while dashed lines refer to the present model. FG2b criterion, $Br = 0$.

The influence of viscous heating on heat transfer performance is also investigated. To do so, the VG2a criterion (fixed flow rate, pumping power, and heat flux) was applied to the following reference configuration: liquid water flowing through a square channel ($\beta = 1$) with sharp corners; $L_0 = 10$ mm; $D_{h,0} = 0.2$ mm; $u_0 = 2$ m/s; $T_w = 30$ °C. Again, the investigated test case is representative of a realistic microchannel application. The heat flux, which is the PEC objective function for the VG2a criterion, and the entropy generation number are evaluated, applying the geometrical constraints of Table 2 as a function of the smoothing radius via Equations (10), (12), (22), and (25). Thus, the influence of both viscous heating and entry region on the average Nusselt number are included in the analysis. In order to show the influence of the Brinkman number Br , related to viscous heating, the same configuration is optimised, imposing $Br_0 = 0$ and $Br_0 = 10^{-3}$, the latter being

consistent with the reference configuration considered. Since the optimisation provided by PEC is based on the first law of thermodynamics and, thus, does not consider the entropy generation, maximisation of a composite objective function, which depends on both PEC and EGN, is considered, following the approach first introduced by Zimparov [52,53].

Figure 7a shows that the effect of the viscous dissipation on the predicted heat flux is actually negligible. Indeed, the Brinkman number is still relatively low and the critical length, at which viscous heat becomes dominant, is much higher than the reference channel length $Pe_0^{-1} L_0/D_{h,0} \simeq 2 \times 10^{-2}$; see Figure 4. On the other hand, Figure 7b shows that the viscous heat affects the entropy generation (particularly when the geometrical restriction is applied to P), even though the predicted trends for $Br_0 = 0$ and $Br_0 = 10^{-3}$ are qualitatively similar. It is interesting to note that the combined objective function to be maximised for the VG2a criterion, defined as $F = q^*/N_T$, is strongly influenced by the presence of the viscous heating: if $Br = 0$, smoothing the corners has a weak influence on F , while an increase of F up to the 6% is observed, under $P^* = 1$ restriction, for the circular duct configuration, if the viscous heating is included (i.e., the Brinkman number is set to its proper value $Br_0 = 10^{-3}$); a maximum of F , which is not predicted in the case where $Br_0 = 0$, is also observed for $\gamma \simeq 0.4$, when $D_h^* = 1$ is applied and $Br_0 = 10^{-3}$. This is quite important since it proves that the viscous heating plays a crucial role in the evaluation of the heat transfer performance of a microchannel device.

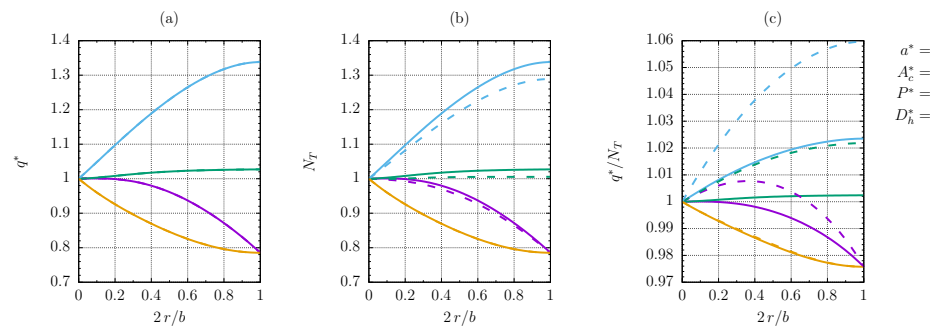


Figure 7. Normalised heat flux (a), entropy generation number due to heat transfer (b), and combined objective function (c), as a function of the non-dimensional smoothing radius. Continuous lines refer to $Br = 0$ (i.e., viscous heating is neglected), dashed lines refer to $Br = 10^{-3}$. VG2a criterion, $Pe_0 = 2.7 \times 10^3$, $L/D_h = 50$, $C_T = 60$, and $\phi_0 = 10^{-1}$.

Once the consistency of the mathematical formulation has been verified with literature models and the need to include both the thermal entry region and the viscous heating for an accurate prediction of the heat transfer performance of microchannels have been proved, the optimization of a real test case is conducted. In particular, we aim at enhancing the performance of an initial square channel with sharp corners. The non-dimensional parameters, which are required by the numerical model and define the reference configuration to be optimised, are listed in Table 6. It can be verified that such parameters are derived via rounding the corresponding values from the following configuration: liquid water at inlet temperature $T_i = 20$ °C flowing with velocity $u_0 = 1.5$ m/s in square microchannels with constant wall temperature $T_w = 30$ °C, hydraulic diameter $D_{h,0} = 180$ μ m, and $L_0 = 1$ cm long. Furthermore, the critical length L_{cr}/D_h , at which the channel is heated by the fluid due to heat generation deriving from viscous dissipation, see Figure 4, is much larger than the reference channel length $L_0/D_{h,0}$, meaning that the considered reference configuration falls inside a reasonable operating condition. The FG1a, FG1b, FG2a, FG2b, VG2a, and VG2b criteria of Table 1 are applied. Results are shown for the four geometrical constraints of Table 2. In practical applications, the constraint to be applied is dictated by the problem. Following [52,53], a combined objective function that depends on both PEC and EGN is considered.

Table 6. Non-dimensional parameters, referred to the reference configuration and required as input by the numerical model.

β	γ_0	$L_0/D_{h,0}$	C_T	ϕ_0	Pe_0	Br_0
1	0	60	30	10^{-2}	1900	10^{-3}

3.2.1. FG1a Criterion

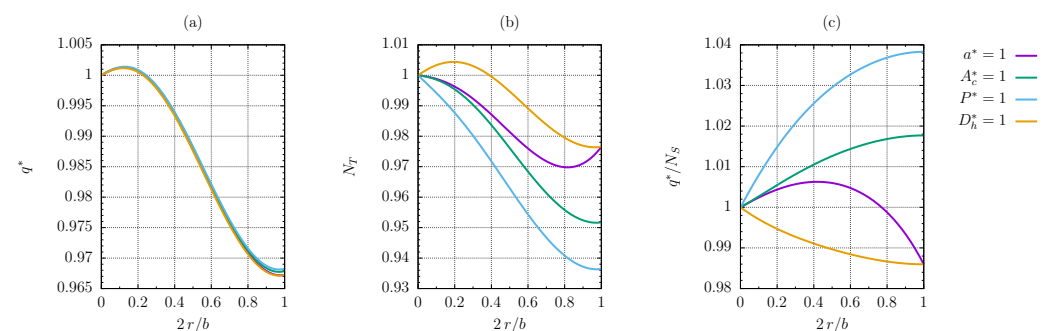
Applying the FG1a criterion requires maximisation of the heat flux q^* at constant flow rate $\dot{m}^* = 1$, and channel length $L^* = 1$. Thus, the resulting composite objective function is defined as

$$F = \frac{q^*}{N_S} \quad (41)$$

so that F , which has to be maximised, will always be equal to 1 for the reference configuration with sharp corners. The straightforward implementation of Equation (10), with $\dot{m}^* = 1$, $L^* = 1$ and Pe , Nu evaluated as a function of the channel cross-section geometry via Equations (33) and (35) provide q^* as a function of γ , while Equations (22), (25) and (26) allow the calculation of N_S . It should be noted that both the Brinkman number and the Peclet number, which are required to compute the coefficients A , B , defined in Equation (11), and the average Nusselt number change with the channel geometry and with some of the PEC objective functions according to

$$Pe = Pe|_0 \frac{\dot{m}^* D_h^*}{A_c^*}, \quad Br = Br|_0 \frac{\dot{m}^{*2}}{A_c^{*2} \Delta T^*} \quad (42)$$

Figure 8a shows the heat flux as a function of the non-dimensional smoothing radius: the predicted heat flux weakly depends on the geometrical constraint, with a maximum always observed for $\gamma \simeq 0.13$; however, a slight dependence of F on the smoothing radius is observed, with variations lower than 4%. The entropy generation number, due to heat transfer, Figure 8b, can be minimised by smoothing the corners, with the best configuration being given by a circular cross-section for P^* , A_c^* , $D_h^* = 1$, while applying restriction $a^* = 1$ gives the minimum of N_T for $\gamma \simeq 0.8$. Since optimisation using either the first or the second law of thermodynamics gives different indications, the analysis of the combined function F is crucial to determine the best compromise. Figure 8c shows that F is maximised for a circular section, i.e., $\gamma = 1$, under constraints $P^* = 1$ and $A_c^* = 1$. On the other hand, the sharp corner design is still the best configuration when the hydraulic diameter is kept constant, while a maximum for $\gamma \simeq 0.43$ is obtained when the smoothing radius is changed at fixed side length a .

**Figure 8.** Normalised heat flux (a), entropy generation number due to heat transfer (b), and combined objective function, Equation (41) (c), as a function of the non-dimensional smoothing radius. Reference configuration defined in Table 6, FG1a criterion.

3.2.2. FG1b Criterion

Applying the FG1b criterion means that the inlet temperature difference ΔT^* must be minimised at constant flow rate, \dot{m}^* , and channel length, $L^* = 1$. Thus, the hybrid objective function is defined as

$$F = (\Delta T^* \cdot N_S)^{-1} \quad (43)$$

It should be noted that the calculation of ΔT^* from Equation (10) is not straightforward because the Nusselt number depends on the Brinkman number, which, in turn, depends on ΔT^* , as demonstrated by Equation (42). Thus, the calculation of ΔT^* is iterated, with the updated value of the Brinkman number used to evaluate the average Nusselt number at each step.

As pointed out for the FG1a criterion, the PEC objective function, which is the inlet temperature difference for FG1b, weakly depends on the imposed geometrical constraint and small variations with the smoothing radius are observed as well, with ΔT^* being minimised for $\gamma \simeq 0.13$, see Figure 9a. Compared to the results for FG1a, a different trend is observed for the entropy generation number N_T : the square section design minimises N_T when $D_h^* = 1$ is applied; a weak decrease of N_T , less than 1%, can be achieved for $\gamma \simeq 0.25$, if $a^* = 1$ or $A_c^* = 1$ is applied; almost a 2% decrease of N_T is achieved for $\gamma \simeq 0.34$ when the smoothing radius is changed at a constant cross-section perimeter. The indications from PEC and EGN are in good agreement. Indeed, the composed objective function, Figure 9c reveals that smoothing the corners with $\gamma \simeq 0.28$ under $P^* = 1$ constraint allows the minimisation of F and, thus, represents the best configuration. However, only a small increment of F is reported, while smoothing the corners worsens the heat transfer performance down to -8% under $a^* = 1$ and $D_h^* = 1$ restrictions.

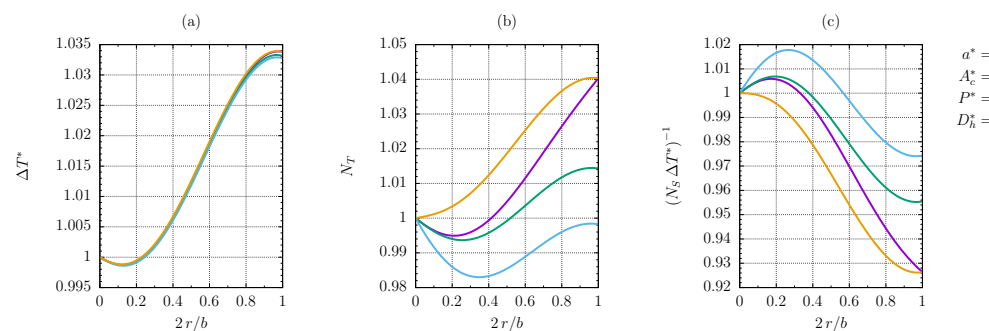


Figure 9. Normalised heat flux (a), entropy generation number due to heat transfer (b), and combined objective function, Equation (43) (c), as a function of the non-dimensional smoothing radius. Reference configuration defined in Table 6, FG1b criterion.

3.2.3. FG2a Criterion

The combined objective function F to be maximised is the same as the one of the FG1a criterion; see Equation (41). Since constraints are applied to W^* and L^* , the normalised flow rate \dot{m}^* must be calculated first using Equation (12). Once \dot{m}^* is known and both the Peclet number and the Brinkman number have been determined through Equation (42), the normalised heat flux can be evaluated via Equation (10) and the entropy generation number can be calculated with Equation (26).

The normalised heat flux, which is the PEC objective function to be maximised for the FG1b criterion, is plotted in Figure 10a versus the smoothing radius. An increment of about 10% of the reference value can be achieved for a circular duct (i.e., $\gamma = 1$) when applying $P^* = 1$. This behaviour can be easily explained: the heat flux increases with the flow rate \dot{m} , which is proportional to the cross-section area A_c , see Equation (7), that, in turn, increases with γ when a restriction on the perimeter of the cross-section is applied. Similarly, setting $A_c^* = 1$ gives a small variation of q with the smoothing radius. Both the restrictions on D_h^* and a^* result in the sharp corner configuration working better in terms of q^* . The entropy generation number due to heat transfer is proportional to the normalised

heat flux exchanged between fluids. Indeed, the trends of N_T , reported in Figure 10b, are similar to the ones of q^* . This, in turn, justifies the behaviour of the composite objective function F , see Figure 10c, which is subjected to small variations (lower than 2%), because it is defined as the ratio between q^* and N_T . The circular duct shape performs best in terms of F for A_c^* , P^* , $D_h^* = 1$, while smoothing the corners up to $\gamma \simeq 0.62$ is convenient for the restriction $a^* = 1$.

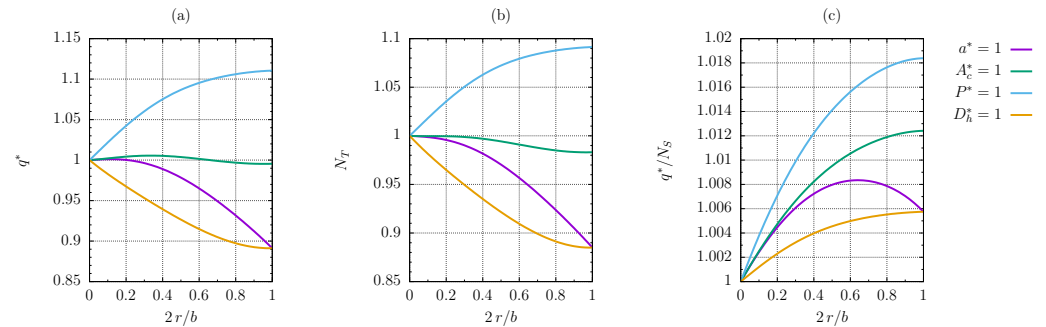


Figure 10. Normalised heat flux (a), entropy generation number due to heat transfer (b), and combined objective function, Equation (41) (c), as a function of the non-dimensional smoothing radius. Reference configuration defined in Table 6, FG2a criterion.

3.2.4. FG2b Criterion

The combined objective function F of the FG2b criterion is the same as the one of FG1b; see Equation (43). Again, constraints are applied to both the pumping power and the channel length, $W^* = 1$ and $L^* = 1$; the heat flux is also known, since $q^* = 1$ for the FG2b criterion. Thus, \dot{m}^* , which is required to estimate ΔT^* , is computed via Equation (12).

The Nusselt number depends on the Brinkman number, which, in turn, depends on the unknown ΔT^* . Thus, the solution ΔT^* of Equation (10) is sought via an iterative method. Once \dot{m}^* and ΔT^* are known, the entropy generation number N_S and the objective function $F = (N_S \Delta T^*)^{-1}$ can be calculated. Figure 11a,b show that the trends of ΔT^* and N_T , that must be minimised, are similar, meaning that observations for the PEC-based optimization can be extended to both EGN and the combined objective function. Indeed, the circular duct shape performs best in terms of ΔT^* , N_T , and F when $P^* = 1$ is applied, with an improvement of 25% in terms of F , while the square section with sharp corners offers better performance when $D_h^* = 1$ or $a^* = 1$ are applied. Smaller variations (+2% of F obtained for $\gamma \simeq 0.4$) are observed when the cross-section area is kept constant, $A_c^* = 1$.

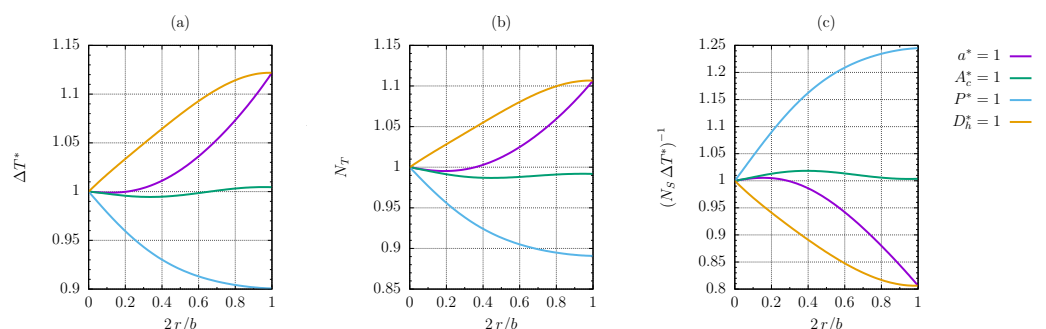


Figure 11. Normalised heat flux (a), entropy generation number due to heat transfer (b), and combined objective function, Equation (43) (c), as a function of the non-dimensional smoothing radius. Reference configuration defined in Table 6, FG2b criterion.

3.2.5. VG2a Criterion

Applying the VG2a criterion entails maximising q^* at fixed ΔT^* , W^* , and \dot{m}^* . The combined objective function for the VG2a criterion is defined by Equation (41). As the normalised channel length L^* is required to estimate the global heat flux q^* , $\dot{m}^* = 1$ and

$W^* = 1$ are set in Equation (12) to derive L^* . Then, the Nusselt number, whose correlation requires the channel length, can be obtained and used to estimate both q^* and N_S .

Comparing Figure 12 to Figure 10, one can observe that results for the VG2a criterion are qualitatively similar to the ones for the FG2a criterion. Indeed, smoothing the corners is profitable when the cross-section perimeter or the cross-section area is fixed with an increment of about 2.7% the reference value of F . A maximum of F is also observed for $\gamma \simeq 0.5$, if $a^* = 1$ is applied. On the other hand, smoothing the corners is not convenient when the hydraulic diameter is constant.

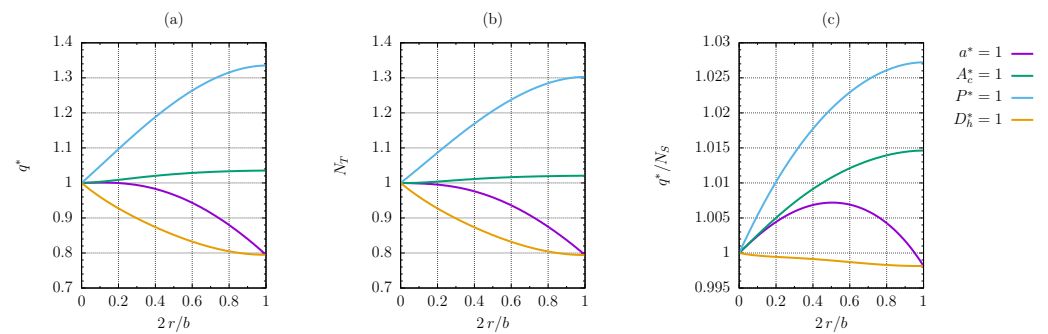


Figure 12. Normalised heat flux (a), entropy generation number due to heat transfer (b), and combined objective function, Equation (41) (c), as a function of the non-dimensional smoothing radius. Reference configuration defined in Table 6, VG2a criterion.

3.2.6. VG2b Criterion

The objective is maximising the function $F = (N_S \Delta T^*)^{-1}$, which is the same as the one defined for the FG1b criterion, with restrictions applied to q^* , \dot{m}^* , and W^* . The normalised channel length and the Peclet number are estimated from Equations (12) and (42). Calculating the unknown ΔT^* requires the iterative solution of Equation (10) since the Nusselt number depends on the Brinkman number Br , which, in turn, changes with ΔT^* .

Figure 13 shows that the considerations made for the FG2b criterion can be extended to the VG2b criterion. Indeed, the circular duct configuration is convenient if $P^* = 1$, with an improvement in F of about 80% (the improvement is less pronounced for the FG2b criterion), while smoothing the corners worsens the performance when $a^* = 1$ or $D_h^* = 1$ is applied. As opposed to FG2b, Figure 13c shows that an improvement of 10%; the reference value of F is also achieved by rounding the corners when $A_c^* = 1$.

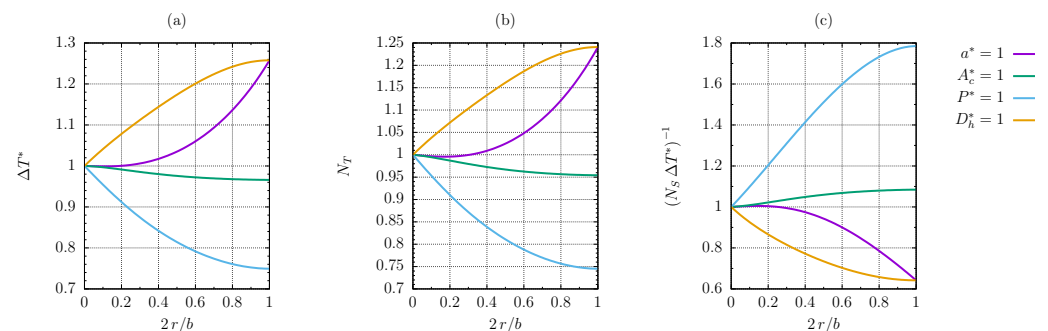


Figure 13. Normalised heat flux (a), entropy generation number due to heat transfer (b), and combined objective function, Equation (43) (c), as a function of the non-dimensional smoothing radius. Reference configuration defined in Table 6, VG2b criterion.

4. Conclusions

This study dealt with the combined optimisation of microchannels of a square cross-section with smoothed corners. The Brinkman–Graetz problem was solved for the laminar flow of a Newtonian fluid with temperature-independent thermophysical properties in a channel with uniform temperature at the walls. The Brinkman numbers investigated

ranged from 0 to 10^{-2} , thus covering both the absence and presence of significant viscous dissipation. The flow and temperature fields were used to compute the Poiseuille and the average Nusselt numbers. The latter was expressed as a function of the average Nusselt number for a zero-Brinkman, developing flow of the Nusselt number for non-negligible viscous dissipation and fully developed flow and of a parameter depending on the smoothing radius of the corners. The critical length of the microchannel was then correlated with the Brinkman number and with the radius of the curvature of the cross-section. This gave the limiting value, beyond which heat flux reverses, going from the fluid to the walls and making the use of the device pointless. It was demonstrated that the correlation for the Nusselt number predicts the numerical results outstandingly up to the critical length. The correlation can, therefore, be used confidently for design purposes by experimentalists and practitioners alike.

The entropy balance was used to obtain the contribution to entropy generation due to either pressure drop or heat transfer and to calculate the corresponding entropy generation number. The Nusselt and Poiseuille numbers were then used to compute the value of the objective function for microchannel optimisation through PEC. The results from PEC were combined with those from second-law analysis (as exemplified by the entropy generation number, EGN) into a single objective function, F , which was plotted as a function of the non-dimensional radius of the curvature of the corners for all the PEC investigated in the case of $Br = 10^{-3}$ and for four different geometrical constraints (fixed characteristic length, fixed hydraulic diameter, fixed heated perimeter, and fixed cross-sectional area). A comparison was made with the outcomes of a previous similar model, [52], where the contribution of the entry region was disregarded and it was found that the results of the latter could be misleading for higher Peclet numbers, both with and without viscous heating, the latter becoming significant in the calculation of the EGN, regardless of the value of Pe .

The results were discussed for every single criterion, with some observations applying to all cases:

- The constrained heated perimeter and cross-sectional area almost invariably exhibit an improvement from the reference configuration when the corners are smoothed. The sole exception is criterion FG1b. The comparison with a standard modelisation in the case of the VG2a criterion proves that viscous heating plays a crucial role, showing that the increase in the objective function is more substantial when viscous dissipation is present, if the constrained heated perimeter and cross-sectional area are considered.
- The constrained characteristic length and hydraulic diameter never yield better results if the corners are smoothed, the FG2a criterion being the only exception; for the FG1a and VG2a criteria, there is a local maximum for in-between values of the smoothing parameter γ corresponding to a minimum improvement of F when the characteristic length is fixed, albeit limited to about 1%;
- Some plots exhibit maxima and minima for some in-between values of the smoothing radius, but the trend is primarily monotonous.

In closing, it is remarked that all results and correlations presented are of general validity and obtained in ranges of the relevant parameters, which fully correspond to real cases, and can, therefore, be used with confidence both for design purposes and experimental validation.

Author Contributions: Conceptualization, M.L. and N.S.; Methodology, M.L. and N.S.; Software, M.L. and N.S.; Validation, M.L. and N.S.; Formal analysis, M.L. and N.S.; Investigation, M.L. and N.S.; Resources, M.L. and N.S.; Data curation, M.L. and N.S.; Writing—original draft, M.L. and N.S.; Writing—review & editing, M.L. and N.S.; Visualization, M.L. and N.S.; Supervision, M.L. and N.S. All authors have read and agreed to the published version of the manuscript.

Funding: This research received no external funding.

Data Availability Statement: Dataset available on request from the authors.

Conflicts of Interest: The authors declare no conflicts of interest.

Abbreviations

The following abbreviations are used in this manuscript:

EGM	Entropy generation minimisation
EGN	Entropy generation number
FG	Fixed Geometry
MFD	Micro-flow device
PEC	Performance evaluation criteria
VG	Variable Geometry

References

- Ohadi, M.; Choo, K.; Dessiatoun, S.; Cetegen, E. *Next Generation Microchannel Heat Exchangers*; Springer Briefs in Applied Sciences and Technology; Springer: New York, NY, USA, 2013. [\[CrossRef\]](#)
- Han, Y.; Liu, Y.; Li, M.; Huang, J. A review of development of micro-channel heat exchanger applied in air-conditioning system. *Energy Proc.* **2012**, *14*, 148–153. [\[CrossRef\]](#)
- Tuckerman, D.; Pease, R.; Guo, Z.; Hu, J.; Yildirim, O.; Deane, G.; Wood, L. Microchannel heat transfer: Early history, commercial applications, and emerging opportunities. In Proceedings of the International Conference on Nanochannels, Microchannels, and Minichannels, Edmonton, AB, Canada, 19–22 June 2011; Volume 2, pp. 739–756. [\[CrossRef\]](#)
- Yu, Z.Q.; Li, M.T.; Cao, B.Y. A comprehensive review on microchannel heat sinks for electronics cooling. *Int. J. Extrem. Manuf.* **2024**, *6*, 022005. [\[CrossRef\]](#)
- Xiong, X.; Li, Y.; Zhao, C.; Yu, W. Recent progress on heat transfer performance and influencing factors of different microchannel heat sinks. *J. Enhanc. Heat Transf.* **2023**, *30*, 71–120. [\[CrossRef\]](#)
- Li, H.; Zou, Z.; Li, H.; Chen, Y.; Fu, C. Thermal performance of a microchannel primary surface recuperator for portable microturbine generators: Design and experimental study. *Appl. Therm. Eng.* **2022**, *206*, 118103. [\[CrossRef\]](#)
- Aydin, O.; Avci, M. Laminar forced convective slip flow in a microduct with a sinusoidally varying heat flux in axial direction. *Int. J. Heat Mass Transf.* **2015**, *89*, 606–612. [\[CrossRef\]](#)
- Lorenzini, M.; Fabbri, G.; Salvigni, S. Performance evaluation of a wavy-fin heat sink for power electronics. *Appl. Therm. Eng.* **2007**, *27*, 969–975. [\[CrossRef\]](#)
- Vishnu, R.; Selvakumar, R.D.; Alkaabi, A.K.; Vengadesan, S. Active vortex generation and enhanced heat transfer in a 3D minichannel by Onsager-Wien effect. *Appl. Therm. Eng.* **2023**, *233*, 121064. [\[CrossRef\]](#)
- Morini, G.L. Viscous heating in liquid flows in micro-channels. *Int. J. Heat Mass Transf.* **2005**, *48*, 3637–3647. [\[CrossRef\]](#)
- Koo, J.; Kleinstreuer, C. Liquid flow in microchannels: Experimental observations and computational analyses of microfluidics effects. *J. Micromech. Microeng.* **2003**, *13*, 568–579. [\[CrossRef\]](#)
- Henning, T.; Brandner, J.; Schubert, K.; Lorenzini, M.; Morini, G. Low-frequency instabilities in the operation of metallic multi-microchannel evaporators. *Heat Transf. Eng.* **2007**, *28*, 834–841. [\[CrossRef\]](#)
- Baek, S.; Bradley, P.E.; Radebaugh, R. Heat transfer coefficient measurement of LN₂ and GN₂ in a microchannel at low Reynolds flow. *Int. J. Heat Mass Transf.* **2018**, *127*, 222–233. [\[CrossRef\]](#)
- Yang, Y.; Chalabi, H.; Lorenzini, M.; Morini, G. The effect on the nusselt number of the nonlinear axial temperature distribution of gas flows through microtubes. *Heat Transf. Eng.* **2014**, *35*, 159–170. [\[CrossRef\]](#)
- Manda, U.; Mazumdar, S.; Peles, Y. Effects of cross-sectional shape on flow and heat transfer of the laminar flow of supercritical carbon dioxide inside horizontal microchannels. *Int. J. Therm. Sci.* **2024**, *201*, 108992. [\[CrossRef\]](#)
- Asim, M.; Mohammad, S.; Kanwal, A.; Uddin, G.M.; Khan, A.A.; Mujtaba, M.; Veza, I.; Kalam, M.; Almomani, F. Comparative study of the parameters affecting the performance of microchannels' heat exchangers: Latest advances review. *Energy Sci. Eng.* **2023**, *11*, 3869–3887. [\[CrossRef\]](#)
- Suzzi, N.; Lorenzini, M. Viscous heating of a laminar flow in the thermal entrance region of a rectangular channel with rounded corners and uniform wall temperature. *Int. J. Therm. Sci.* **2019**, *145*, 106032. [\[CrossRef\]](#)
- Suzzi, N.; Lorenzini, M. Numerical Investigation of Thermally Developing and Fully Developed Electro-Osmotic Flow in Channels with Rounded Corners. *Fluids* **2021**, *6*, 22. [\[CrossRef\]](#)
- Herwig, H.; Hausner, O. Critical view on “new results in micro-fluid mechanics”: An example. *Int. J. Heat Mass Transf.* **2003**, *46*, 935–937. [\[CrossRef\]](#)
- Morini, G.L.; Lorenzini, M.; Colin, S.; Geoffroy, S. Experimental investigation of the compressibility effects on the friction factor of gas flows in microtubes. In Proceedings of the 4th International Conference on Nanochannels, Microchannels and Minichannels, ICNMM2006, Limerick, Ireland, 19–21 June 2006; Volume 2006 A, pp. 411–418. [\[CrossRef\]](#)
- Çetin, B.; Yazıcıoğlu, A.G.; Kakaç, S. Slip-flow heat transfer in microtubes with axial conduction and viscous dissipation—An extended Graetz problem. *Int. J. Therm. Sci.* **2009**, *48*, 1673–1678. [\[CrossRef\]](#)
- Vocale, P.; Morini, G.L.; Spiga, M. Dilute gas flows through elliptic microchannels under H₂ boundary conditions. *Int. J. Heat Mass Transf.* **2014**, *71*, 376–385. [\[CrossRef\]](#)

23. Barletta, A.; Magyari, E. The Graetz–Brinkman problem in a plane-parallel channel with adiabatic-to-isothermal entrance. *Int. Commun. Heat Mass Transf.* **2006**, *33*, 677–685. [\[CrossRef\]](#)
24. Dong, X.; Liu, X. Multi-objective optimization of heat transfer in microchannel for non-Newtonian fluid. *Chem. Eng. J.* **2021**, *412*, 128594. [\[CrossRef\]](#)
25. Lorenzini, M.; Daprá, I.; Scarpi, G. Heat Transfer for a Giesekus Fluid in a Rotating Concentric Annulus. *Appl. Therm. Eng.* **2017**, *122*, 118–125. [\[CrossRef\]](#)
26. Kiyasatfar, M. Convective heat transfer and entropy generation analysis of non-Newtonian power-law fluid flows in parallel-plate and circular microchannels under slip boundary conditions. *Int. J. Therm. Sci.* **2018**, *128*, 15–27. [\[CrossRef\]](#)
27. Bayareh, M. An overview of non-Newtonian nanofluid flow in macro- and micro-channels using two-phase schemes. *Eng. Anal. Bound. Elem.* **2023**, *148*, 165–175. [\[CrossRef\]](#)
28. Colin, S.; Lalonde, P.; Caen, R. Validation of a second-order slip flow model in rectangular microchannels. *Heat Transf. Eng.* **2004**, *25*, 23–30. [\[CrossRef\]](#)
29. Su, L.; Yang, Y. Convective Heat Transfer and Entropy Generation Analysis in Elliptic Microchannels. *ASME J. Heat Mass Transf.* **2024**, *146*, 021004. [\[CrossRef\]](#)
30. Sadr, R.; Yoda, M.; Zheng, Z.; Conlisk, A. An experimental study of electro-osmotic flow in rectangular microchannels. *J. Fluid Mech.* **2004**, *506*, 357–367. [\[CrossRef\]](#)
31. Geri, M.; Lorenzini, M.; Morini, G. Effects of the Channel Geometry and of the Fluid Composition on the Performance of DC Electro-osmotic Pumps. *Int. J. Therm. Sci.* **2012**, *55*, 114–121. [\[CrossRef\]](#)
32. Shamshiri, M.; Khazaeli, R.; Ashrafizaadeh, M.; Mortazavi, S. Electroviscous and thermal effects on non-Newtonian liquid flows through microchannels. *ASME J. Non-Newton. Fluid Mech.* **2012**, *173*–174, 1–12. [\[CrossRef\]](#)
33. Shit, G.; Mondal, A.; Sinha, A.; Kundu, P. Electro-osmotic flow of power-law fluid and heat transfer in a micro-channel with effects of Joule heating and thermal radiation. *Phys. A Stat. Mech. Its Appl.* **2016**, *462*, 1040–1057. [\[CrossRef\]](#)
34. Al-Rjoub, M.; Roy, A.; Ganguli, S.; Banerjee, R. Assessment of an active-cooling micro-channel heat sink device, using electro-osmotic flow. *Int. J. Heat Mass Transf.* **2011**, *54*, 4560–4569. [\[CrossRef\]](#)
35. Al-Rjoub, M.; Roy, A.; Ganguli, S.; Banerjee, R. Improved flow rate in electro-osmotic micropumps for combinations of substrates and different liquids with and without nanoparticles. *J. Electron. Packag. Trans.* **2015**, *137*, 021001. [\[CrossRef\]](#)
36. Michelsen, M.L.; Villadsen, J. The Graetz problem with axial heat conduction. *Int. J. Heat Mass Transf.* **1974**, *17*, 1391–1402. [\[CrossRef\]](#)
37. Basu, T.; Roy, D.N. Laminar heat transfer in a tube with viscous dissipation. *Int. J. Heat Mass Transf.* **1985**, *28*, 699–701. [\[CrossRef\]](#)
38. Aparecido, J.B.; Cotta, R.M. Thermally developing laminar flow inside rectangular ducts. *Int. J. Heat Mass Transf.* **1990**, *33*, 341–347. [\[CrossRef\]](#)
39. Lee, P.S.; Garimella, S.V. Thermally developing flow and heat transfer in rectangular microchannels of different aspect ratios. *Int. J. Heat Mass Transf.* **2006**, *49*, 3060–3067. [\[CrossRef\]](#)
40. Filali, A.; Khezzar, L.; Siginer, D.; Nemouchi, Z. Graetz problem with non-linear viscoelastic fluids in non-circular tubes. *Int. J. Therm. Sci.* **2012**, *61*, 50–60. [\[CrossRef\]](#)
41. Barışık, M.; Yazıcıoğlu, A.G.; Çetin, B.; Kakaç, S. Analytical solution of thermally developing microtube heat transfer including axial conduction, viscous dissipation, and rarefaction effects. *Int. Commun. Heat Mass Transf.* **2015**, *67*, 81–88. [\[CrossRef\]](#)
42. Webb, R.L.; Kim, N.H. *Principles of Enhanced Heat Transfer*; Taylor and Francis: New York, NY, USA, 2004.
43. Webb, R.; Eckert, E. Application of rough surfaces to heat exchanger design. *Int. J. Heat Mass Transf.* **1972**, *15*, 1647–1658. [\[CrossRef\]](#)
44. Bergles, A.; Blumenkrantz, A.; Taborek, J. Performance Evaluation Criteria for enhanced heat transfer surfaces. In Proceedings of the International Heat Transfer Conference 5, Tokyo, Japan, 3–7 September 1974.
45. Bejan, A. The concept of irreversibility in heat exchanger design: Counterflow heat exchangers for gas-to-gas applications. *J. Heat Transf.* **1977**, *99*, 374–380. [\[CrossRef\]](#)
46. Bejan, A. *Entropy Generation through Heat and Fluid Flow*; Wiley: New York, NY, USA, 1982.
47. Bejan, A. Thermodynamic optimization of geometry in engineering flow systems. *Exergy Int. J.* **2001**, *1*, 269–277. [\[CrossRef\]](#)
48. Yilmaz, M.; Sara, O.N.; Karsli, S. Performance evaluation criteria for heat exchangers based on second law analysis. *Exergy Int. J.* **2001**, *1*, 278–294. [\[CrossRef\]](#)
49. Saenen, T.; Baelmans, M. Size effects of a portable two-phase electronics cooling loop. *Appl. Therm. Eng.* **2013**, *50*, 1174–1185. [\[CrossRef\]](#)
50. Stevens, T.; Baelmans, M. Optimal pressure drop ratio for micro recuperators in small sized gas turbines. *Appl. Therm. Eng.* **2008**, *28*, 2353–2359. [\[CrossRef\]](#)
51. Karathanassis, I.K.; Papanicolaou, E.; Belessiotis, V.; Bergeles, G.C. Multi-objective design optimization of a micro heat sink for Concentrating Photovoltaic/Thermal (CPVT) systems using a genetic algorithm. *Appl. Therm. Eng.* **2013**, *59*, 733–744. [\[CrossRef\]](#)
52. Zimparov, V. Extended performance evaluation criteria for enhanced heat transfer surfaces: Heat transfer through ducts with constant wall temperature. *Int. J. Heat Mass Transf.* **2000**, *43*, 3137–3155. [\[CrossRef\]](#)
53. Zimparov, V. Extended performance evaluation criteria for enhanced heat transfer surfaces: Heat transfer through ducts with constant heat flux. *Int. J. Heat Mass Transf.* **2001**, *44*, 169–180. [\[CrossRef\]](#)

54. Zimparov, V.; Vulchanov, N. Performance evaluation criteria for enhanced heat transfer surfaces. *Int. J. Heat Mass Transf.* **1994**, *37*, 1807–1816. [[CrossRef](#)]
55. Petkov, V.; Zimparov, V.; Bergles, A. Performance evaluation of ducts with non-circular shapes and laminar fully developed flow. *Int. Rev. Chem. Eng.* **2012**, *4*, 379–391.
56. Petkov, V.; Zimparov, V.; Bergles, A. Performance evaluation of ducts with non-circular shapes: Laminar fully developed flow and constant wall temperature. *Int. J. Therm. Sci.* **2014**, *79*, 220–228. [[CrossRef](#)]
57. Ray, S.; Misra, D. Laminar fully developed flow through square and equilateral triangular ducts with rounded corners subjected to H1 and H2 boundary conditions. *Int. J. Therm. Sci.* **2010**, *49*, 1763–1775. [[CrossRef](#)]
58. Chakraborty, S.; Ray, S. Performance optimisation of laminar fully developed flow through square ducts with rounded corners. *Int. J. Therm. Sci.* **2011**, *50*, 2522–2535. [[CrossRef](#)]
59. Lorenzini, M.; Morini, G. Single-phase, Laminar Forced Convection in Microchannels with Rounded Corners. *Heat Transf. Eng.* **2011**, *32*, 1108–1116. [[CrossRef](#)]
60. Lorenzini, M.; Suzzi, N. The Influence of Geometry on the Thermal Performance of Microchannel Heat Sinks with Viscous Dissipation. *Heat Transf. Eng.* **2016**, *37*, 1096–1104. [[CrossRef](#)]
61. Suzzi, N.; Lorenzini, M. Performance assessment of electro-osmotic flow of rectangular microchannels with smoothed corners. *Phys. Fluids Conf. Ser.* **2023**, *2648*, 012069. [[CrossRef](#)]
62. Wibulswas, P. Laminar Flow Heat Transfer in Non-Circular Ducts. Ph.D. Thesis, University College London, London, UK, 1966.

Disclaimer/Publisher's Note: The statements, opinions and data contained in all publications are solely those of the individual author(s) and contributor(s) and not of MDPI and/or the editor(s). MDPI and/or the editor(s) disclaim responsibility for any injury to people or property resulting from any ideas, methods, instructions or products referred to in the content.